Assessment of the shock adsorption properties of bike helmets: a numerical/experimental approach

Massimiliano Bocciarelli[1], Valter Carvelli[1], Stefano Mariani[2,3*], Matteo Tenni[4]

[1] Politecnico di Milano, Dipartimento di Architettura, Ingegneria delle Costruzioni e Ambiente Costruito,
Piazza L. da Vinci 32, 20133 Milano (Italy)

[2] Politecnico di Milano, Dipartimento di Ingegneria Civile e Ambientale,
Piazza L. da Vinci 32, 20133 Milano (Italy)

[3] Politecnico di Milano, E4Sport - Engineering for Sport Laboratory,
Piazza L. da Vinci 32, 20133 Milano (Italy)

[4] MET S.p.A.
Via Piemonte 373, 23018 Talamona (Italy)

* Corresponding author:
Tel.: +39-02-2399-4279
Fax: +39-02-2399-4300
e-mail: stefano.mariani@polimi.it

E-mail addresses: massimiliano.bocciarelli@polimi.it (Massimiliano Bocciarelli)
valter.carvelli@polimi.it (Valter Carvelli)
stefano.mariani@polimi.it (Stefano Mariani)
matteo@met-helmets.com (Matteo Tenni)

Assessment of the shock adsorption properties of bike helmets: a numerical/experimental approach

In this paper, a numerical and experimental study of the shock absorption properties of bike helmets is presented. Laboratory compression and tensile tests were carried out on samples of expanded polystyrene (EPS) and polycarbonate (PC), respectively constituting the internal shock absorption layer and the external hard shell of composite helmets. The measured responses of the two materials were then exploited to calibrate the relevant elasto-plastic constitutive models, adopted in full-scale finite element analyses of a helmet subject to standardized impacts. The simulations allowed assessing the time evolution of the acceleration measured inside the headform (according e.g. to EN 1078, 2012) and the failure mechanisms of the helmet, if any, as induced by the localization of plastic deformations.

Keywords: helmets; impacts; traumatic brain injury (TBI); numerical modelling.

1. Introduction

Sport injuries have been recently the focus of several research works. With specific reference to mild traumatic brain injuries (mTBIs) caused by accidental head impacts that may occur during sport events or training, both the short-term effects on athletes' performance and the long-term rehabilitation, with possible chronical diseases and difficulties to fully recover, were of concern. To frame relevant studies, a precise definition of mTBI was provided in (Arciniegas, 2011): "*Mild TBI describes a specific injury event; this event produces acute disruptions of brain function and, at the more severe end of mTBI, brain structure. Acute disruptions of cerebral function reflect neurobiological processes that, for the most part, are both transient and reversible*". Definitions of acute and persistent post-concussive symptoms were also reported in the same study.

From paediatric subjects all the way up to professional athletes, it is nowadays perceived that mTBIs can be largely reduced if appropriately designed helmets are always

worn. Most of the published studies focused primarily on sports like American football and ice hockey, see e.g. (Wilcox *et al*. 2014, Kuhn *et al.* 2017). During field tests, helmets instrumented with inertial micro-devices (see also Andena *et al.* 2016, Cobb *et al.* 2018) were adopted to quantitatively assess repeated impacts in terms of head/helmet linear and angular accelerations, and then correlate data with the emergence of mTBIs. In order to combine information related to the time evolution of the accelerations, not only in terms of their peak values, indices like HIC (Head Injury Criterion), GSI (Gadd Severity Index), and the Wayne State Tolerance curve were adopted. As stated in (Greenwald et al. 2008), these quantitative measures are all apt to foresee the occurrence of a severe TBI, whereas measures for mTBIs are still somehow lacking.

To further understand the importance of safety-related issues, initiatives published by the Centre for Disease Control and Prevention in USA and by the Istituto Superiore di Sanità in Italy (Giustini *et al.* 2005) can be mentioned, among others. They revealed the enormous amount of head injuries happening every year, in many instances with underage people involved. In ski parks such traumatic events resulted in a 10% probability of mTBIs before the mandate of wearing ski helmets. For cycling, the lack in several countries of laws enforcing to wear helmets does not help to face the risks associated to sharing the roads with vehicles.

As far as TBI issues and helmet beneficial effects are concerned, in agreement with the simple classification proposed in (Andena *et al.* 2016) sports can be subdivided into two main categories: a former one, including e.g. cycling and alpine skiing, characterized by medium-high energy impacts caused by accidental events seldom happening; a latter one, including e.g. American football and ice hockey, characterized instead by low energy impacts that can be repeated several times during a match. In this work, protective helmets for the first sports category are studied. Even though bike and

ski helmets are typically made of very similar polymeric materials and are all constituted by a rigid external shell and by a soft inner liner, they are subjected to impacts of different energy levels and, on top of all, have to work under very different environmental conditions. For comfort needs, bike helmets have a geometry more complex than ski ones, with ventilation openings that may worsen their shock adsorption capability.

The impact behaviour of bike helmets was studied in (Cripton *et al.* 2014) showing that, not surprisingly, the helmets always provide a significant benefit independently of drop height, falling orientation and criterion adopted to quantify the cushioning effect in laboratory tests, see also (Forero Rueda *et al.* 2011, Ganpule *et al.* 2012). Though not exhaustive due to the limited number of experiments, in (Smith *et al.* 2015) an interesting comparison was reported between composite helmets, like those here investigated, and the football and hockey ones. Allowing for both direct and indirect loadings, due to the contact with the stricken surface and to the head/neck kinematics, it was shown for the combination of geometry and materials adopted that acceleration values may result to be much larger for bike helmets; this provides the background for the emergence of more severe TBI effects, and paves the way to look for performance improvements (Milne *et al.* 2012).

Regarding the cushioning effect, an investigation was proposed in (Tinard *et al.* 2011) for motorcyclist helmets, specifically focusing on standard dynamic laboratory testing. Differently than that study, here reference is purposely made to international standards like (EN 1078, 2012), to assess the aforementioned overall cushioning effect measured during shock tests. Hence, a predictive model of a headform wearing the helmet, hitting an anvil after a guided free fall from a standardized height, was developed. Due to the ventilation openings, rather complicated and localized failure mechanisms can be triggered in the helmet, requiring a sophisticated and refined simulation strategy to

link drop features and acceleration peaks. In the simulations, the constitutive laws for the two materials constituting the external shell (polycarbonate, PC) and the internal liner (expanded polystyrene, EPS) of the composite helmet were calibrated on the basis of their response measured through an experimental campaign.

To address all these points, the paper is organized as follows. In Section 2 the main results of the experimental campaign on materials samples are summarized. Section 3 provides details of the constitutive modelling for EPS and PC, tuned on the basis of the main features of the materials behaviour highlighted by experiments. In Section 4, along with results at the helmet scale some features of the structural analysis are discussed, to get insights into the foreseen accuracy of the numerical simulations. Finally, in Section 5 some concluding remarks are gathered, along with suggestions for possible improvements to better mimic the reality in case of accidental impacts.

2. Materials: experimental tests and results

As discussed in the Introduction, sport helmets have a composite structure, with a hard external shell and a foamed inner liner. The experimental characterization was therefore provided independently for the materials of the two parts, namely for PC and EPS.

Mechanical tests at room temperature were carried out to investigate the effect of the loading rate on the compressive and tensile responses of the materials; in this regard, PC was assumed to have a symmetric behaviour under tension and compression (Tvergaard and Needleman 2008), so that only tensile tests were conducted. An MTS 358 Bionix testing machine was used for all the tests, with a load cell of 25 kN; tests were under displacement control, to also allow measuring the post-peak softening response of the materials preceding failure. During tensile tests on EPS and PC, the longitudinal deformation in the specimens was continuously recorded by an MTS 632.85F-05

extensometer (gauge length 25 mm, accuracy class 0.5, strain range from +7% to -6%). To avoid damages to the instrumentation during compression tests on EPS, the extensometer was not adopted, and the deformation was computed by means of the machine stroke, assuming the strain state to be uniform in the materials samples. During the same compression tests, a spherical hinge allowed a correction of small misalignments of the specimen sides due to imperfections in the casting stage.

For both the loading conditions, at least three specimens were tested; average values of the (nominal) longitudinal stress and scattering around them were then estimated, considering the real (imperfection-affected) cross-section area of the specimens.

2.1 Expanded polystyrene

An EPS with a density of 95 kg/m^3 and a bead diameter of around 2 mm, supplied by Sunpor, was considered. Specimens for uniaxial tension tests were casted into a dog-bone shape, with the following main geometrical features: width at the grip zone 40 mm, width of the free length 25 mm, thickness 32 mm, total length 180 mm, and free length 50 mm (adapted from ISO 527, 2012). Specimens were gripped using a low rugosity contact metal surface of the wedge grip, and avoiding the crush of EPS by setting a proper pressure level of the hydraulic grips.

The compression response was instead measured through prismatic samples, featuring a cross-section of 50×50 mm^2 and a thickness of 32 mm (adapted from ISO 604, 2002). PTFE (PolyTetraFluoroEthylene) sheets were positioned between specimen and steel supports, to reduce the influence of friction and allow the lateral expansion of the specimen on the contact surfaces.

To assess the rate-dependent response of EPS, different values of the longitudinal strain rate were adopted: under tension, $\dot{\varepsilon} = 0.2$ s^{-1} and 2.0 s^{-1}; under compression

$\dot{\varepsilon} = 0.1 s^{-1}$ and $1.0 s^{-1}$. Though slightly different in the two testing configurations due to technical reasons, such values allowed to investigate the possible change in the response for rates differing by one order of magnitude. Since the strain rate values of interest in case of impacts can be as large as $50 - 100$ s^{-1}, a rate dependent model was then calibrated to provide appropriate values of the EPS properties for the simulations of the whole helmet, see Section 3.1 and also (Andena *et al.* 2015; Andena *et al.* 2018).

The tensile stress vs strain response of EPS is depicted in Figure 1 for $\dot{\varepsilon} = 0.2$ s^{-1} and $\dot{\varepsilon} = 2.0$ s^{-1}. The curves reported in these graphs are the responses of different specimens, and therefore representative of the scattering expected in the test outcomes. The plots for $\dot{\varepsilon} = 0.2$ s^{-1} (Figure 1a) show an initial (almost linear) elastic branch, which is followed by a hardening one that covers one third of the whole strain range till failure; the hardening, or deviation from linearity, is shown to decrease by increasing the strain rate. In these graphs, the values of stress and strain are given in a non-dimensional form, to better focus on the main features of the response; σ_0 and ε_0 are therefore meant as reference values for the longitudinal stress and strain, that allow catching the trend in the response and the pertinent scattering. The values of stress at yielding and/or at failure are shown explicitly in other graphs, to assess their dependence on the strain rate.

The aforementioned dependence on the strain rate of the ultimate strength and of the Young's modulus in the initial elastic regime, are shown in Figure 2. As far as the elastic property is concerned, it looks rather rate-independent with no significant variations in the experimental scatter bands. The average strength is instead increased by around 6-7% when the strain rate is increased by one order of magnitude; also the scattering around the mean gets increased at the higher strain rate, but this additional feature was not accounted for in the deterministic, rate dependent numerical model to be discussed in Section 3.1.

The compressive response is shown in Figure 3. The typical stress-strain curve shape is reported (see e.g. Ling *et al.* 2018, Mosleh *et al.* 2017): a (rather limited) linear elastic range is followed by a relatively large plateau, featuring a sensibly decreased stiffness in comparison with the initial stage, after which the stress increases sharply as a consequence of foam densification. As depicted in Figure 4, the yield strength (represented as positive, even if in compression), smaller than the tensile failure one, shows a 20% enhancement by increasing the strain rate. The compressive elastic modulus is a bit more than one half of the value in tension, and it gets slightly increased with the strain rate. Concerning this difference between the measured values of E_t and E_c, very similar results were reported in (Walter *et al.* 2008) for a closed-cell thermoplastic (PVC) foam with a comparable density of 100 kg/m^3; as discussed in (Walter *et al.* 2008), such a bi-modularity is rather common for polymeric foams, and "*is associated with the nonlinear nature of the elastic responses in tension and compression*", see also (Menges and Knipschild, 1982).

2.2 Polycarbonate

Due to the symmetric response of PC, compression tests were not conducted to avoid all the issues related to the buckling of thin specimens. The tested PC had a density of 1200 kg/m^3 and was supplied by General Electric. The specimens had a prismatic geometry featuring (adapted from ISO 527, 2012): total length 300 mm, free length 150 mm, width 25 mm, and thickness 0.8 mm. The PC itself was also used for the tabs of length 75 mm, glued at both ends of each specimen on the gripping zones. The adopted strain rates in the tests were the same considered for EPS.

The typical stress vs. strain behaviour, as resulted for all the strain rates, is depicted in Figure 5. Similarly to EPS, the linear elastic response is followed by a stage slightly deviating from linearity, up to failure for a value of the stress larger than the

reference σ_0 one by 50%, and around twice that at yielding (so, at deviation from linearity).

The measured properties of PC showed a negligible dependence on the strain rate in the considered range; therefore, relevant results are not reported.

3. Materials modelling

Some details of the numerical modelling of EPS and PC are next detailed. Reference is made to the data collected with the experimental tests; a preliminary calibration of the models allowed to attain the numerical/experimental matching shown in the following. Since micromechanical features at yielding and failure were not specifically collected during the experimental activity, primarily aiming at the calibration of the constitute models to be adopted at the helmet scale, a purely phenomenological approach was adopted.

All the simulations were carried out with the general purpose finite element (FE) code Abaqus (Simulia 2017). To avoid a broad discussion on numerical aspects rather than materials and helmet performance, only the relevant features of the simulations are presented here.

3.1 Expanded polystyrene

Test outcomes reported in Section 2.1 highlighted some typical features of the response of expanded polymeric materials to loadings, see e.g. (Di Landro *et al.* 2002, Song *et al.* 2005, Ouellet *et al.* 2006, Caserta *et al.* 2010, Kiernan and Gilchrist 2010, Mills 2010, Arezoo *et al.* 2013, Chen *et al.* 2015, Duncan *et al.* 2016). Specifically, it can be observed that: under tension, a smooth evolution from the initial elastic regime to the subsequent hardening one occurs, till a sudden failure of the foam due to decohesion; under compression, after the characteristic plateau, showing a slightly increasing stress

level, a remarkable hardening shows up, due to the densification and the relevant compressive crushing of the foam; the Young's modulus is higher under tensile loading, vice-versa the ultimate strength is higher under compressive loading; strengths are influenced by the deformation rate, with positive strain rate effects; elastic moduli, both in tension and compression, are marginally affected by the deformation rate. Furthermore, within the inspected range the strain rate dependence of fracture toughness looks marginal, even though collected data cannot give an overview of the possible embrittlement of the foam at higher strain rates.

All these features can be taken in due account at the helmet scale, via a phenomenological rate-dependent elasto-plastic constitutive model featuring a pressure-dependent yield function with strain hardening up to saturation.

Concerning the different elastic stiffness under tensile and compressive stress states, the feature was disregarded in the constitutive modelling. To be able to match the speed of compressive waves travelling inside the composite helmet and inducing the failure of EPS by crushing, the compressive Young's modulus was taken as a reference in the simulations. As the main interest in this work was on modelling the highly nonlinear post-yielding response of EPS, featuring plastic strain-induced failure mechanisms in the foam at finite deformations, the initial elastic response was supposed to have a minor effect.

As far as the yielding behaviour is concerned, a rather standard way to account for the pressure-sensitive response of materials is through the Drucker-Prager model. In its standard formulation for isotropic materials (see e.g. Zienkiewicz and Taylor 2000), yielding is activated when the stress state attains the following frame-invariant locus, see Figure 6:

$$\varphi = q - p\ \tan\beta - c = 0 \qquad (1)$$

where: $q = \sqrt{\frac{3}{2}\boldsymbol{s}:\boldsymbol{s}}$ is proportional to the second invariant of the stress deviator $\boldsymbol{s} = \boldsymbol{\sigma} - p\boldsymbol{I}$ (where symbol ':' denotes the inner product of second order tensors, namely $\boldsymbol{s}:\boldsymbol{s} = s_{ij}s_{ji}$, with $i,j = 1,2,3$); $\boldsymbol{\sigma}$ is the stress tensor; $p = \frac{1}{3}\mathrm{tr}\boldsymbol{\sigma}$ is the hydrostatic stress (as tr denotes the trace of the second order tensor $\boldsymbol{\sigma}$); $\boldsymbol{I}$ is the second order identity tensor; β is the friction angle; c is the cohesion, i.e. the material strength at $p = 0$. As this model was developed for cohesive-frictional materials (typically soils), the terminology might look somehow misleading for polymeric foams. At any rate, a major feature of this yield condition is the capability of providing different strength levels under tension and compression. Accordingly, the amplitudes of the tensile and compressive yield strengths σ_y^C and σ_y^T (both positive here) are linked to each other through:

$$\sigma_y^T = \frac{1-\frac{1}{3}\tan\beta}{1+\frac{1}{3}\tan\beta}\sigma_y^C \tag{2}$$

where the role played by the slope β of the yield law (1) clearly emerges. Enhanced versions of this model were proposed to also account for tensile or compressive cut-off and further provide a limitation to the elastic domain, see e.g. (de Souza Neto *et al.* 2008, Simo and Hughes 1998). As such enhanced models would not add much in terms of the capability to describe the experimentally observed failure modes of the helmets, and would also require the calibration of additional constitutive parameters (besides β and c) through ad-hoc laboratory tests, they were not considered in the present study.

Another important feature of pressure-sensitive materials is represented by dilation. Standard materials modelling (see de Souza Neto *et al.* 2008) is based on associative flow rules, meaning that, at each point of a body, plastic deformations develop at yielding so as to fulfil the relationship:

$$\dot{\boldsymbol{\varepsilon}}^p = \dot{\Lambda}\frac{\partial \varphi}{\partial \boldsymbol{\sigma}} \tag{3}$$

where: $\dot{\boldsymbol{\varepsilon}}^p$ is the rate of change of the plastic deformation tensor $\boldsymbol{\varepsilon}^p$ (which sums up to the elastic one $\boldsymbol{\varepsilon}^e$ to provide the total strain tensor $\boldsymbol{\varepsilon}$); $\dot{\Lambda}$ is a proportionality factor, termed plastic multiplier, that is to be determined from the Kuhn-Tucker complementarity conditions locally defining whether an unloading or a loading path is followed by the stress state (details can be found, e.g. in Simo and Hughes 1998); $\frac{\partial \varphi}{\partial \boldsymbol{\sigma}}$ defines the direction of plastic flow in the hyperspace of the strain tensor components. A compressive yield strength higher than the tensile one induces dilation, in case of associative flow rules (i.e. for $\alpha = \beta$ in Figure 6): the development of plastic deformations then gives rise to an increase of the material volume, due to $\mathrm{tr}\dot{\boldsymbol{\varepsilon}}^p > 0$. The other way around, the macroscopic response of foamed materials at yielding is characterized by crushing of the walls of each cell and densification. To limit this contradictory response of the model for EPS, a null dilation was obtained by adopting a non-associative flow rule featuring $\alpha = 0$. This would lead to numerical issues in FE simulations if an implicit time integrator were adopted (see Bathe 1996, de Souza Neto *et al.* 2008), as linked to an algorithmic updating procedure requiring the inversion of a non-symmetric matrix. Since the focus of this work is on the response to impacts, which cause the propagation of stress waves in the helmet, an explicit time integrator (Bathe 1996) was adopted; hence, detrimental effects numerically induced by the non-associative behaviour of EPS were of no concern. It is also to highlight that, even if material dilation was dropped, the elasto-plastic model is still incapable of addressing the compaction of the foam under compressive stresses. The plastic strain-induced failure feature of the software Abaqus was thus exploited to remove the material (actually, the elements) in the regions where a critical plastic strain threshold

was attained, avoiding possible locking effects due to the mentioned incapability of describing foam compaction.

Strain rate effects on the yield strength in compression were modelled according to the Nagy law, see e.g. (Zhang *et al.* 1998, Scarpa *et al.* 2004, Andena *et al.* 2019, Chen *et al.* 2015), which reads:

$$\frac{\sigma_y^C}{\sigma_{y,0}^C} = \left(\frac{\dot{\varepsilon}}{\dot{\varepsilon}_0}\right)^n \tag{4}$$

where: $\sigma_{y,0}^C$ is the strength measured at a reference strain rate $\dot{\varepsilon}_0$, while σ_y^C is the same strength measured at a different strain rate $\dot{\varepsilon}$; n is a specific model index. Index n is often assumed to be a linear function of the strain ε; here, by referring to the stress level at the inception of plasticity only, n is instead assumed to be a constant. According to the results reported in Fig. 4(a), it turned out that $n = 0.06$; though deformation-independent, this value fits well the ranges reported e.g. in (Andena *et al.* 2019) for other foams with a similar density.

Such rate effects on the material strength were allowed for up to the strain-rate regime typically reported in the failing regions of the helmet, with values not exceeding $50 - 100$ s^{-1}. One main question arising with this procedure is whether the rate-dependence measured in the range $\dot{\varepsilon} \leq 10$ s^{-1} (see Section 2.1) can be extended up to the strain rate interval of interest in case of impacts. Former investigations on amorphous polymers (see, e.g. Mulliken and Boyce 2006, D'Mello *et al.* 2012) and on foams (Pellegrino *et al.* 2015, Krundaeva *et al.* 2016) showed that, up to strain rates of the order of 100 s^{-1}, there are no abrupt regime-transitions in the material response. Hence, the value of n tuned at low strain rates was assumed valid also for the analysis of impacts on the helmet. This assumption may affect the accuracy of the results in comparison to experimental data relevant to real tests featuring different anvil geometries and falling

orientations, overall resulting in different interactions between impactor and ventilation openings, especially if very localized failure modes are expected to be triggered.

When a local failure process is modelled, an overall softening effect shows up, and the structural stiffness gets globally reduced; from the computational viewpoint, this represents a serious issue linked to ill-posedness (Bazant and Cedolin 2010) that results in a pathological dependence of the modelled response on the adopted space discretization. Within the aforementioned explicit time integration environment, this problem can be prevented or largely limited through a so-called regularization procedure based on fracture energy (Comi and Perego 2001); independently of the characteristic size of the finite elements in the failing regions, the regularization assures that failure occurs by locally dissipating the proper material-dependent amount of energy $\mathcal{G}_F$. Such procedure allowed modelling the whole failure mechanism, and a direct comparison with the experimental outcomes.

The obtained predictions are plotted in Figure 7 for a value of the friction angle $\beta = 30°$, under tensile and compressive loadings. Unlike the experimental results of Section 2.1, the comparison is here detailed with reference to the full specimen behaviour in terms of load P vs. imposed displacement u, to show the interaction between material and structural effects. Accounting for the measured (and expected) dispersion of the experimental data, it can be seen that the proposed model well matched all the relevant features of the elastic and post-yielding behaviour of EPS under compression. In tension the model was not able to catch the hardening branch shown by the specimens, and a kind of perfectly plastic response preceded failure by decohesion. It must be anyway noted that the post-yielding phase at a constant load was actually induced by the counteracting effects of EPS hardening and cross-section thinning due to specimen deformation.

3.2 Polycarbonate

As mentioned, PC was assumed to have a symmetric response under tensile and compressive loadings. After serigraphy, PC showed the following properties (see Bauwens-Crowet *et al.* 1974, Wendlandt *et al.* 2005, Srivastava *et al.* 2010, Lu and Li 2011, Cao *et al.* 2016, Ikeshima *et al.* 2018, Matadi Boumbimba *et al.* 2018): a smooth evolution of the stress-strain response close to yielding, leading to a slight deviation from linearity in the post-elastic regime; a limited ductility, with a deformation at failure on the order of $2-3$ times the value at yielding; a low dependence of its elastic and strength properties on the stain rate, up to a threshold well above the rates of deformation characteristic of impacts on bike helmets.

For a purely phenomenological modelling of PC, an elastic perfectly plastic response was assumed, with yielding captured by the von Mises condition (hence assuming $\sigma_y^T = \sigma_y^C$, or $\beta = 0$ in Eq. 1). Accordingly, the mentioned deviation from linearity after the triggering of plasticity was disregarded. Alike EPS, associative flow rules and a fracture energy-regularized local failure modelling were adopted, the latter driven by the accumulation of localized plastic deformations. To provide failure modelling on the safe side, with a possible slight underestimation of the real failure load, rate effects were neglected; it is therefore expected that the simulated acceleration peaks due to the impacts on helmet, can be somehow affected too.

The modelled overall response of the PC specimens to the tensile test is shown in Figure 8; results are once again compared with the recorded experimental data. According to the above mentioned simplifications, the numerical response is linear up to yielding at a load P of around 300 N. Next, the assumed perfectly plastic response of PC cannot be evidenced since plastic deformations localize, leading to global softening characterized by a decreasing value of P and then failure.

4. Full-scale analysis of impacts on helmets

To assess the capability of the numerical procedure to mimic the response of bike helmets under impact loadings, reference was made to prescriptions in (EN 1078, 2012). After a free fall from a pre-defined height providing a velocity v at impact, to give protection for any possible location of the impact itself it is specified that the peak acceleration measured inside a standardized headform (see EN 960, 2006 and Figure 9) must not exceed the critical threshold of $250g$, g being the gravity acceleration. This acceleration is strictly correlated to the capacity of the helmet to absorb the impact energy, and the more the said energy is absorbed in the helmet by the development of permanent (plastic) deformations the lower the amount of energy transmitted to the head.

Two different types of anvil, or stricken objects, were considered: a flat one and a kerbstone one, both made of steel. For these two anvil types, the mentioned velocity at impact is respectively set as v_f =5.42 m/s or v_k =4.57 m/s, where subscripts f and k stand for flat and kerbstone. As far as the orientation of the helmet and the relevant impact location are concerned, as shown in Figure 10 three different configurations were considered: a frontal impact against the kerbstone striker; a back impact against the kerbstone striker; a lateral impact against the flat striker. As requested by the standard and to check the outcomes relevant to the most dangerous scenarios, the impacts against the kerbstone anvil were assumed to happen in correspondence of some ventilation openings. In Figure 10 a headform of size 535 according to (EN 960, 2006), helmet and anvil are displayed with the corresponding space discretizations. The handled helmet is a former commercial product, whose geometry was partially modified by increasing the size of ventilation openings and by removing some strengthening parts, in order to purposely reduce its load-bearing capacity and assess the spreading of damage if the helmet locally fails.

After some preliminary analyses, aimed at optimizing the space discretization to attain accuracy in the results within a reasonable computing time, a mesh with an average element size of 4 mm for the helmet and of 6 mm for headform and anvil was selected, overall consisting of 395,544 tetrahedral elements and 18,308 shell elements (see below), featuring 294,858 degrees of freedom. Due to the difference in thickness between the external PC layer and the inner EPS liner, the PC outer skin was assumed to behave like a shell; this assumption allowed to largely simplify the meshing procedure and to reduce the computational cost of each analysis.

The dynamic analyses were performed also at the helmet level by adopting an explicit time integration procedure, with a lumped mass matrix and allowing for large deformation effects. A general contact algorithm was adopted to model the surface interaction between the head and the helmet, and between the helmet and the striker; a friction coefficient equal to 0.1 was assumed in both the cases, though materials interacting are different on the helmet side. For both PC and EPS, damage was locally modeled as an internal variable that monotonically increases with plastic deformation; as soon as the critical threshold of $0.7 - 0.8$ of the equivalent plastic strain was attained, failure was triggered by exploiting the Abaqus *element deletion* provision, which allowed to remove FEs from the mesh when fully damaged.

Concerning the mechanical properties of EPS and PC, the same constitutive modeling of Section 3 was adopted. Parameter values, allowing the rather good agreement between experimental and numerical results at the specimen level, were assumed in the real conditions characterizing the tests on the helmet. Accordingly and as already discussed in Section 3.1, the bi-modular elastic behavior of EPS was disregarded to simplify the analysis, as the major test outcome is governed by the crushing of the foam in compression.

For the frontal impact, an experimentally measured time history of the acceleration of the headform was used to validate the approach and check model accuracy. Figure 11 shows a comparison between experimental and numerical results, in terms of the whole time evolution of the amplitude of the acceleration of the headform, so not only in terms of the characteristic peak value. In this graph and in the following ones reporting the acceleration histories, the raw numerical data are provided without any filtering of high-frequency oscillations that might affect the peak values and also the shape of the time histories. Such high-frequency oscillations were due to the reverberation of the impact-induced waves in each helmet layer, and to the unilateral contact between the model parts. Furthermore, acceleration histories were scaled by the threshold value $\bar{a} = 250g$, and time intervals were scaled by a characteristic value $t_{ref} = 5$ ms, corresponding in most of the cases to the attainment of the peak acceleration. The results in terms of the final helmet damage state are reported in Figure 12: a main damaged region is shown to take place where the helmet hit the striker. However, the induced local crack did not result to be a part-through one, as proved by an acceleration peak not exceeding $100g$, which meant that the headform did not get in contact with the striker.

In the case of the back impact, the results obtained are reported in terms of the headform acceleration in Figure 13, and in terms of the final damage pattern in Figure 14. With such impact configuration, the confined compression of PC and EPS due to the relative motion of headform and anvil, induced a localized failure mode in the back of the helmet. Hence, the striker could get in contact with the headform, inducing the upturn of the acceleration graph at the end of the analysis. It is shown that the helmet was initially able to dissipate energy inside the EPS liner, since the acceleration never exceeded the value of 50-60g; only when the failure mode spread in regions surrounding the (as said,

purposely enlarged) openings, a penetration of the anvil occurred and the metal-metal contact gave rise to a wave leading to the measured acceleration growth.

In the case of the lateral impact, the results obtained are reported again in terms of the headform acceleration in Figure 15, and of the final damage pattern in Figure 16. For this falling configuration, the model predicted a diffused damage in the EPS, but the striker could not directly hit the headform due to its flat shape. The acceleration peak resulted to be much larger than that occurring in the frontal case, attaining values close to the critical threshold set by the standards.

It thus appeared that, while the acceleration peak alone can provide a qualitative measure of the requested impact-carrying capacity of the helmet independently of anvil shape and falling orientation, only a deeper understanding and quantification of the dynamic mechanical properties of materials and an accurate modelling of the helmet geometry can allow improving the helmet performance for the foreseen cushioning purposes.

5. Conclusion

In this work, we presented and discussed a numerical tool to predict the performance of bike helmets exposed to impacts, as foreseen e.g. in (EN 1078, 2012). Accurate forecasts of the cushioning properties of a helmet were obtained by first testing the materials constituting the helmet itself (polycarbonate for the outer shell and expanded polystyrene for the inner liner), so as to select and calibrate the most appropriate constitutive models for both of them.

The numerical model, once validated at the helmet level, can be used for the optimization of the helmet geometry with the aim of attaining the appropriate impact-carrying capacity without detrimentally affecting the overall comfort provided by the ventilation openings. Some recent activities tried to better frame the kind of impact that

helmets can experience on the basis of reasonable or most probable falls of both pediatric and adult athletes, see e.g. (Bourdet et al. 2012, Koncan et al. 2016), and correlate them with the standard prescriptions. In future studies, these results will be accounted for to assess how the measure of the helmet cushioning performance can be affected.

To further improve the mentioned predictive capabilities of the model a more extensive experimental campaign is foreseen, to collect data on the strength and toughness properties of the materials within ranges of the strain rate closer to those characterizing the failure mechanisms in the impacted helmet.

Acknowledgements

Financial support to this work was provided by Met S.p.A., which is gratefully acknowledged. SM also acknowledges the funding of project *Safer Helmets* by Fondazione Cariplo.

References

L. Andena, S. Aleo, F. Caimmi, F. Briatico-Vangosa, S. Mariani, S. Tagliabue, A. Pavan. "Modelling the effects of the structure of athletics tracks on their cushioning properties", *Sports Engineering*, under review, 2018.

L. Andena, F. Briatico-Vangosa, E. Cazzoni, A. Ciancio, S. Mariani, A. Pavan. "Modeling of shock absorption in athletics track surfaces", *Sports Engineering*, 18, pp. 1-10, 2015.

L. Andena, F. Caimmi, L. Leonardi, A. Ghisi, S. Mariani, F. Braghin. "Towards Safer Helmets: characterisation, modelling and monitoring", *Procedia Engineering*, 147, pp. 478-483, 2016.

L. Andena, F. Caimmi, L. Leonardi, M. Nacucchi, F. De Pascalis, "Compression of polystyrene and polypropylene foams for energy absorption applications: A combined mechanical and microstructural study", *Journal of Cellular Plastics*, 55, pp. 49-72, 2019.

D.B. Arciniegas, "Clinical electrophysiologic assessments and mild traumatic brain injury: State-of-the-science and implications for clinical practice", *International Journal of Psychophysiology*, 82, pp. 41-52, 2011.

S. Arezoo, V.L. Tagarielli, C.R. Siviour, N. Petrinic, “Compressive deformation of Rohacell foams: Effects of strain rate and temperature”, *International Journal of Impact Engineering*, 51, pp. 50-57, 2013.

K.-J. Bathe, “Finite Element Procedures”, Prentice-Hall, Englewood Cliffs, NJ, USA, 1996.

C. Bauwens-Crowet, J.M. Ots, J.C. Bauwens, “The strain-rate and temperature dependence of yield of polycarbonate in tension, tensile creep and impact tests”, *Journal of Materials Science*, 9, pp. 1197-1201, 1974.

Z.P. Bazant, L. Cedolin, “Stability of Structures: Elastic, Inelastic, Fracture and Damage Theories”, World Scientific Publishing Co., Singapore, 2010.

N. Bourdet, C. Deck, R.P. Carreira, R. Willinger, “Head impact conditions in the case of cyclist falls”, *Proceedings of the Institution of Mechanical Engineers, Part P: Journal of Sports Engineering and Technology*, 226, pp. 282-289, 2012.

K. Cao, X. Ma, B. Zhang, Y. Wang, Y. Wang, “Tensile behavior of polycarbonate over a wide range of strain rates”, *Materials Science and Engineering A*, 527, pp. 4056-4061, 2010.

G. Caserta, U. Galvanetto, L. Iannucci, “Static and Dynamic Energy Absorption of Aluminum Honeycombs and Polymeric Foams Composites”, *Mechanics of Advanced Materials and Structures*, 17, pp. 366-376, 2010.

W. Chen, H. Hao, D. Hughes, Y. Shi, J. Cui, Z.-X. Li, “Static and dynamic mechanical properties of expanded polystyrene”, *Materials & Design*, 69, pp. 170-180, 2015.

B.R. Cobb, A.M. Tyson, S. Rowson, “Head acceleration measurement techniques: Reliability of angular rate sensor data in helmeted impact testing”, *Proceedings of the Institution of Mechanical Engineers, Part P: Journal of Sports Engineering and Technology*, 232, pp. 176-181, 2018.

C. Comi, U. Perego, “Fracture energy based bi-dissipative damage model for concrete”, *International Journal of Solids and Structures*, 38, pp. 6427-6454, 2001.

P.A. Cripton, D.M. Dressler, C.A. Stuart, C.R. Dennison, D. Richards, “Bicycle helmets are highly effective at preventing head injury during head impact: Head-form accelerations and injury criteria for helmeted and unhelmeted impacts”, *Accident Analysis and Prevention*, 70, pp. 1-7, 2014.

L. Di Landro, G. Sala, D. Olivieri, “Deformation mechanisms and energy absorption of polystyrene foams for protective helmets”, *Polymer Testing*, 21, pp. 217-228, 2002.

E.A. de Souza Neto, D. Peric, D.R.J. Owen, “Computational Methods for Plasticity: Theory and Applications”, John Wiley & Sons Ltd, Chichester, UK, 2008.

R.J. D'Mello, S. Guntupalli, L.R. Hansen, A.M. Waas, “Dynamic axial crush response of circular cell honeycombs”, *Proceedings of the Royal Society A: Mathematical, Physical and Engineering Science*, 468, pp. 2981-3005, 2012.

O. Duncan, L. Foster, T. Senior, A. Alderson, T. Allen, “Quasi-static characterisation and impact testing of auxetic foam for sports safety applications”, *Smart Materials and Structures*, 25, 054014, 2016.

EN 960, “Headforms for use in the testing of protective helmets”, 2006.

EN 1078, “Helmets for pedal cyclists and for users of skateboards and roller skates”, 2012.

M.A. Forero Rueda, L. Cui, M.D. Gilchrist, “Finite element modelling of equestrian helmet impacts exposes the need to address rotational kinematics in future helmet designs”, *Computer Methods in Biomechanics and Biomedical Engineering*, 14, pp. 1021-1031, 2011.

S. Ganpule, L. Gu, A. Alai, N. Chandra, “Role of helmet in the mechanics of shock wave propagation under blast loading conditions”, *Computer Methods in Biomechanics and Biomedical Engineering*, 15, pp. 1233-1244, 2012.

M. Giustini, A. Pitidis, G. Fondi, “Sistema SIMON – Sorveglianza degli incidenti in montagna”, Istituto Superiore di Sanità, report OS/AMPP/RT/267, 2005 (in Italian).

R.M. Greenwald, J.T. Gwin, J.J. Chu, and J.J. Crisco, “Head impact severity measures for evaluating mild traumatic brain injury risk exposure”, *Neurosurgery*, 62, pp. 789-798, 2008.

D. Ikeshima, A. Yonezu, L. Liu, “Molecular origins of elastoplastic behavior of polycarbonate under tension: A coarse-grained molecular dynamics approach”, *Computational Materials Science*, 145, pp. 306-319, 2018.

ISO 527-1, “Plastics - Determination of tensile properties - Part 1: General principles”. 2012.

ISO 604, “Plastics - Determination of compressive properties”, 2002.

S. Kiernan, M.D. Gilchrist, “Towards a virtual functionally graded foam: Defining the large strain constitutive response of an isotropic closed cell polymeric cellular solid”, *International Journal of Engineering Science*, 48, pp. 1373-1386, 2010.

D.A. Koncan, R. Zemek, T.B. Hoshizaki, “Performance of children and adult alpine helmets under characteristic falling conditions”, *Procedia Engineering*, 147, pp. 578-583, 2016.

A. Krundaeva, G. De Bruyne, F. Gagliardi, W. Van Paepegem, “Dynamic compressive strength and crushing properties of expanded polystyrene foam for different strain rates and different temperatures”, *Polymer Testing*, 55, pp. 61-68, 2016.

E.N. Kuhn, J.H. Miller, B. Feltman, A.K. Powers, D. Sicking, J.M. Johnston Jr, “Youth helmet design in sports with repetitive low- and medium-energy impacts: a systematic review”, *Sports Engineering*, 20, pp. 29-40, 2017.

C. Ling, J. Ivens, P. Cardiff, M.D. Gilchrist, “Deformation response of EPS foam under combined compression-shear loading. Part I: Experimental design and quasi-static tests”, *International Journal of Mechanical Sciences*, 144, pp. 480–489, 2018.

Y.B. Lu, Q.M. Li, “Dynamic behavior of polymers at high strain-rates based on split Hopkinson pressure bar tests”, *International Journal of Impact Engineering*, 38, pp. 41-50, 2011.

R. Matadi Boumbimba, M. Coulibaly, Y. Peng, E.K. N’souglo, K. Wang, P. Gerard, “Investigation of the impact response of PMMA-based nano-rubbers under various temperatures”, *Journal of Polymer Research*, 25, 76, 2018.

G. Menges, F. Knipschild, “Stiffness and Strength-Rigid Plastic Foams,” in Mechanics of Cellular Plastics, N. C. Hilyard ed., Macmillan, New York, 1982.

N.J. Mills, “Deformation mechanisms and the yield surface of low-density, closed-cell polymer foams”, *Journal of Materials Science*, 45, pp. 5831-5843, 2010.

G. Milne, C. Deck, R.P. Carreira, Q. Allinne, R. Willinger, “Development and validation of a bicycle helmet: assessment of head injury risk under standard impact conditions”, *Computer Methods in Biomechanics and Biomedical Engineering*, 15, pp. 309-310, 2012.

Y. Mosleh, J. Vander Sloten, B. Depreitere, J. Ivens, “Novel Composite Foam Concept for Head Protection in Oblique Impacts”, *Advanced Engineering Materials*, 19, 1700059, 2017.

A.D. Mulliken, M.C. Boyce, “Mechanics of the rate-dependent elastic–plastic deformation of glassy polymers from low to high strain rates”, *International Journal of Solids and Structures,* 43, pp. 1331-1356, 2006.

S. Ouellet, D. Cronin, M. Worswick, “Compressive response of polymeric foams under quasi-static, medium and high strain rate conditions”, *Polymer Testing,* 25, pp. 731-743, 2006.

A. Pellegrino, V.L. Tagarielli, R. Gerlach, N. Petrinic, “The mechanical response of a syntactic polyurethane foam at low and high rates of strain”, *International Journal of Impact Engineering,* 75, pp. 214-221, 2015.

F. Scarpa, L.G. Ciffo, J.R. Yates, “Dynamic properties of high structural integrity auxetic open cell foam”, *Smart Mater. Struct.,* 13, pp. 49-56, 2004.

J.C. Simo, T.J.R. Hughes, “Computational Inelasticity”, Volume 7 of Interdisciplinary Applied Mathematics, Springer-Verlag Inc., New York, NY, USA, 1998.

Simulia, “Abaqus 2017 User Manual”, Dassault Systèmes, Vélizy-Villacoublay (France), 2017.

T.A. Smith, P.D. Halstead, E. McCalley, S.A. Kebschull, S. Halstead, J. Killeffer, “Angular head motion with and without head contact: implications for brain injury”, *Sports Engineering,* 18, pp. 165-175, 2015.

B. Song, W.W. Chen, S. Dou, N.A. Winfree, J.H. Kang, “Strain-rate effects on elastic and early cell-collapse responses of a polystyrene foam”, *International Journal of Impact Engineering,* 31, pp. 509-521, 2005.

V. Srivastava, S.A. Chester, N.M. Ames, L. Anand, “A thermo-mechanically-coupled large-deformation theory for amorphous polymers in a temperature range which spans their glass transition”, *International Journal of Plasticity,* 26, pp. 1138-1182, 2010.

V. Tinard, C. Deck, N. Bourdet, R. Willinger, “Motorcyclist helmet composite outer shell characterisation and modelling”, *Materials & Design,* 32, pp. 3112-3119, 2011.

V. Tvergaard, A. Needleman, “An analysis of thickness effects in the Izod test”, *International Journal of Solids and Structures,* 45, pp. 3951-3966, 2008.

T.R. Walter, A.W. Richards, G. Subhash, “A Unified Phenomenological Model for Tensile and Compressive Response of Polymeric Foams”, *ASME. J. Eng. Mater. Technol.*,131, 011009-011009-6, 2008.

M. Wendlandt, T.A. Tervoort, U.W. Suter, “Non-linear, rate-dependent strain-hardening behavior of polymer glasses”, *Polymer*, 46, pp. 11786-11797, 2005.

B.J. Wilcox, J.G. Beckwith, R.M. Greenwald, J.J. Chu, T.W. McAllister, L.A. Flashman, A.C. Maerlender, A.-C. Duhaime, J.J. Crisco, “Head impact exposure in male and female collegiate ice hockey players”, *Journal of Biomechanics*, 47, pp. 109-114, 2014.

J. Zhang, N. Kikuchi, V. Li, A. Yee, G. Nusholtz, “Constitutive modeling of polymeric foam material subjected to dynamic crash loading”, *International Journal of Impact Engineering*, 21, pp. 369-386, 1998.

O.C. Zienkiewicz, R.L. Taylor, “The Finite Element Method: Solid Mechanics”, 5th ed., Vol. 2, Butterworth-Heinemann, Oxford, 2000.

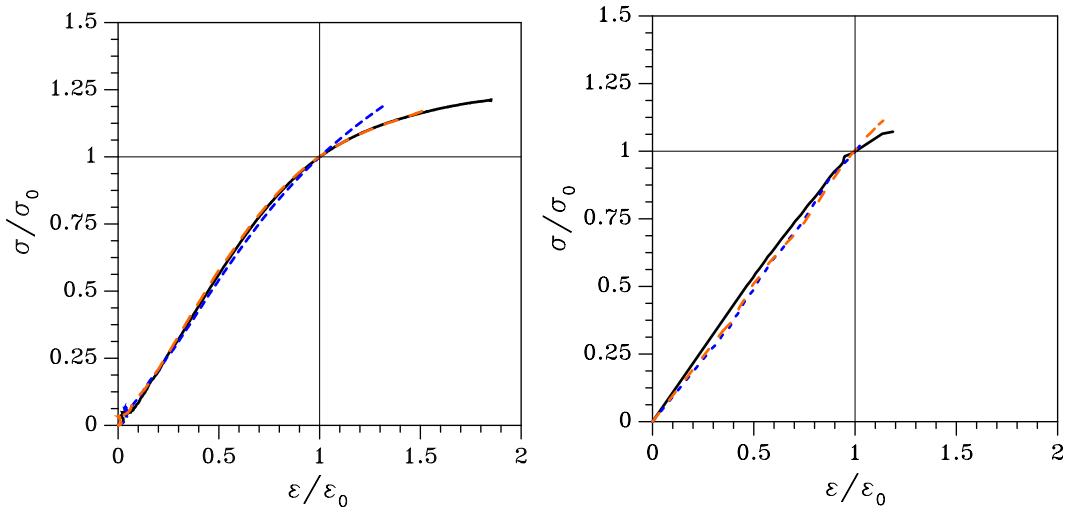

Figure 1. EPS, tensile tests at (a) $\dot{\varepsilon}$ =0.2 s^{-1} and (b) $\dot{\varepsilon}$ =2 s^{-1}: nondimensional stress-strain responses of the tested specimens.

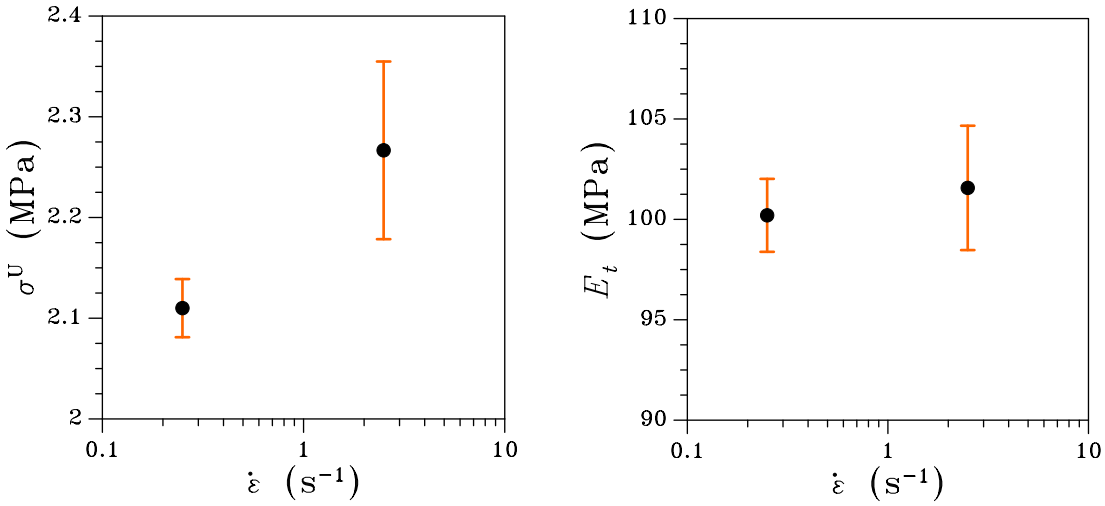

Figure 2. EPS, tensile tests: effect of the strain rate $\dot{\varepsilon}$ on (left) the ultimate strength σ^U, and (right) the tensile Young's modulus E_t.

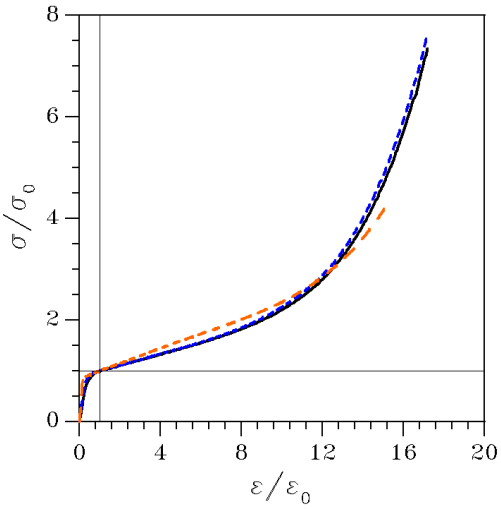

Figure 3. EPS, compressive tests at $\dot{\varepsilon} = 0.1$ s^{-1}: nondimensional stress-strain response of three specimens.

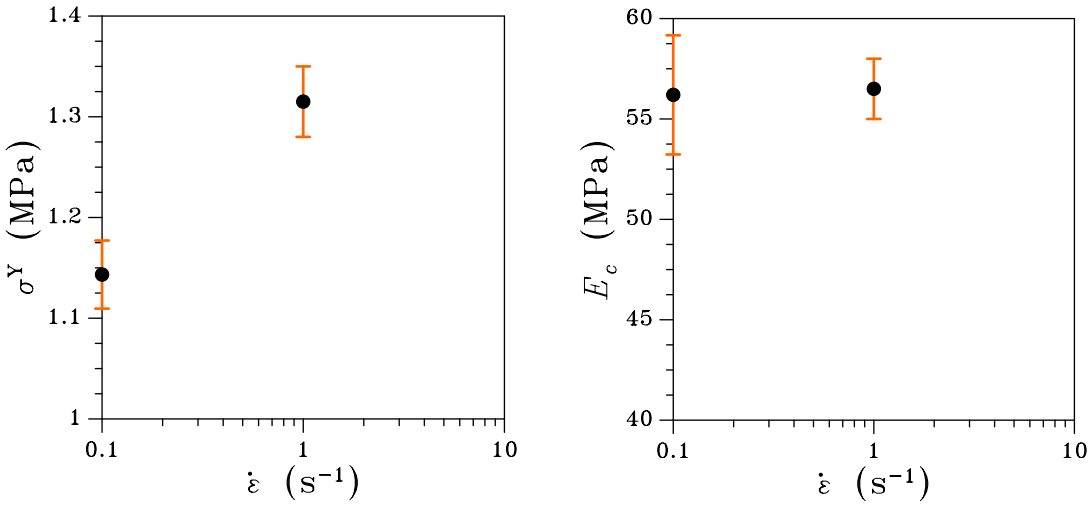

Figure 4. EPS, compressive tests: effect of the strain rate $\dot{\varepsilon}$ on (left) the yield strength σ^{Y}, and (right) the compressive Young's modulus E_c.

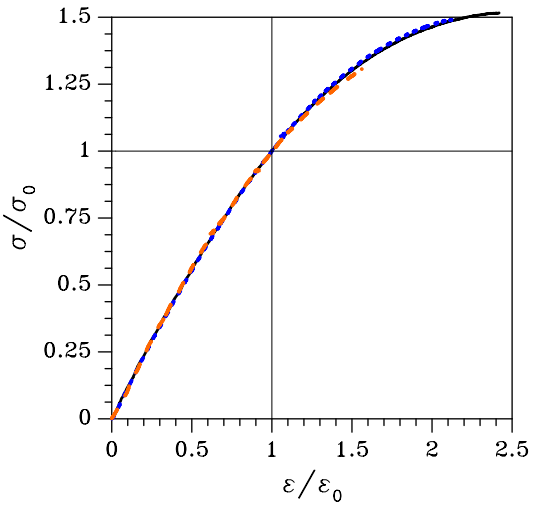

Figure 5. PC, tensile tests at $\dot{\varepsilon} = 0.2\ s^{-1}$: nondimensional stress-strain response of three specimens.

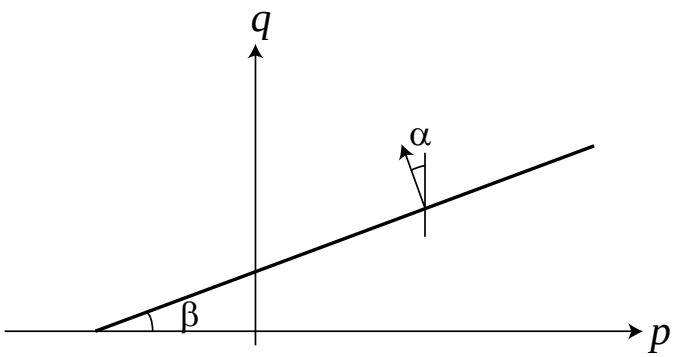

Figure 6. EPS: Drucker-Prager yield surface in the meridional $p - q$ plane, and notation.

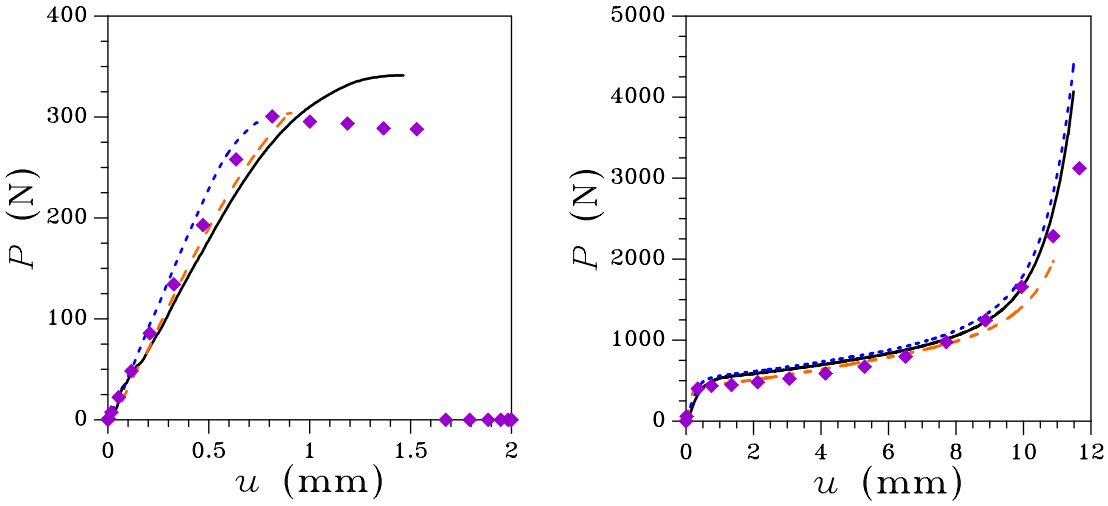

Figure 7. EPS: numerically modelled (symbols) vs. experimentally measured (lines) response, under (left) tensile loading at $\dot{\varepsilon}$ =0.2 s^{-1} and (right) compressive loading at $\dot{\varepsilon}$ =0.1 s^{-1}.

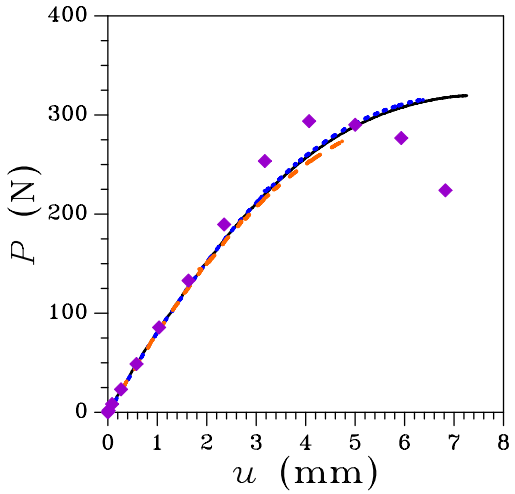

Figure 8. PC: numerically modelled (symbols) vs. experimentally measured (lines) response, under tensile loading at $\dot{\varepsilon} = 0.2\ s^{-1}$.

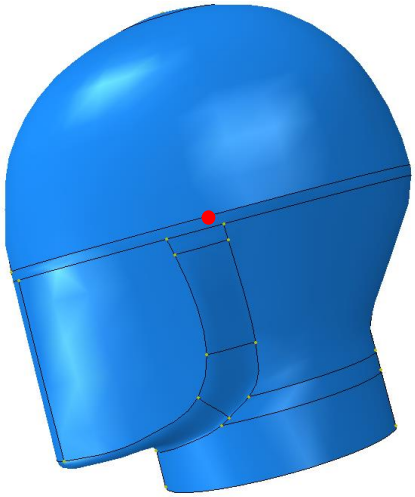

Figure 9. Geometrical model of the headform; the red dot represents the location where the acceleration time histories were recorded in the analyses.

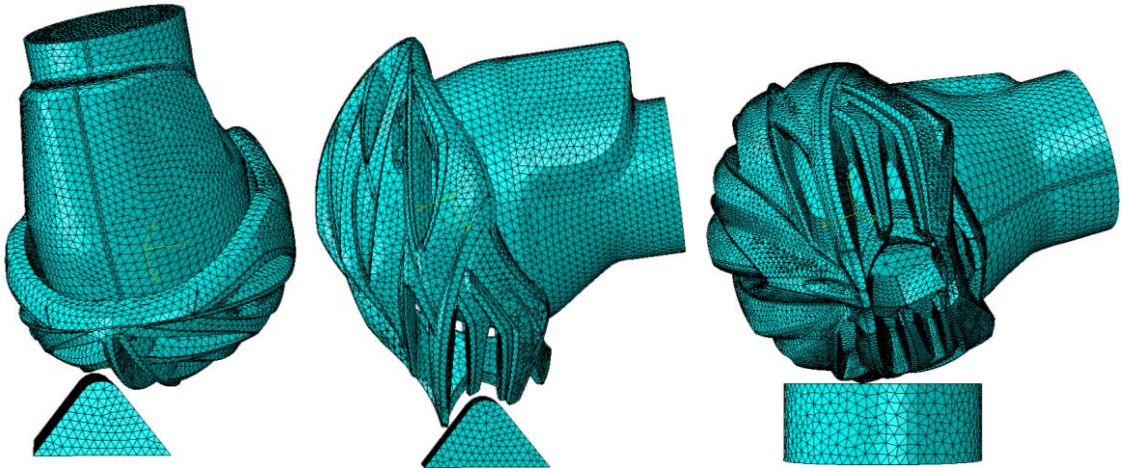

Figure 10. Finite element discretizations adopted to simulate the three types of impact (from left to right: frontal, back and lateral) between the bike helmet and the anvils.

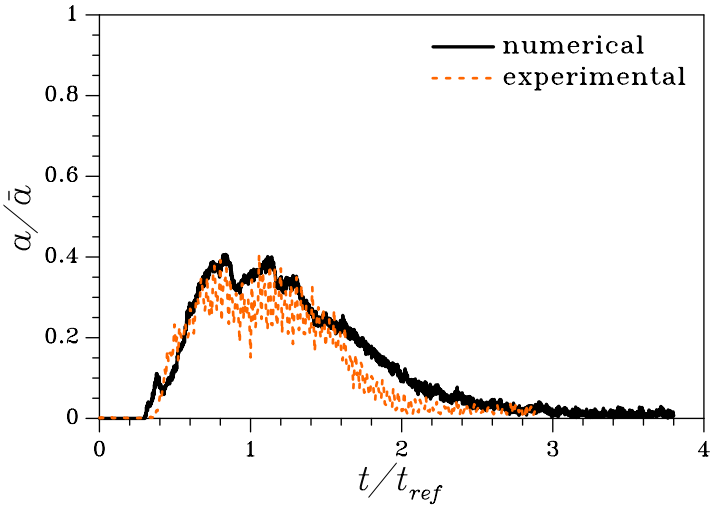

Figure 11. Frontal impact: comparison between numerical and experimental acceleration histories of the headform.

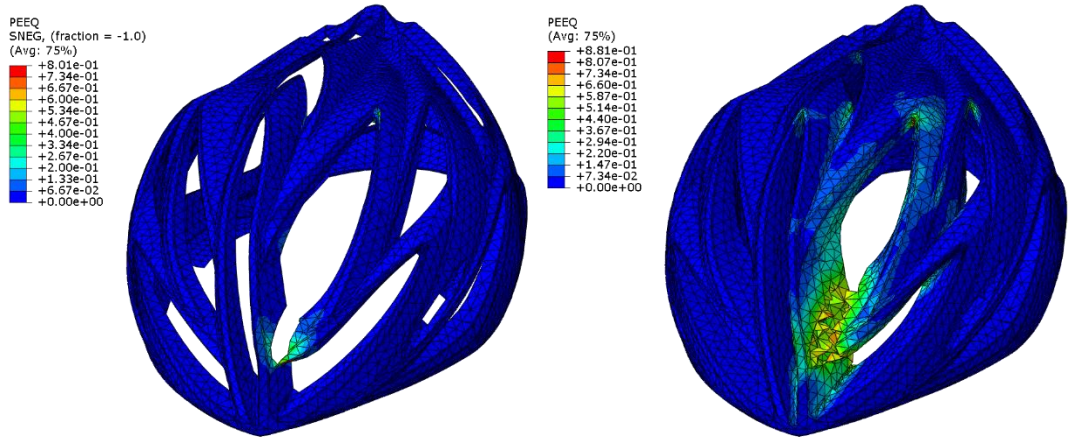

(a) (b)

Figure 12. Frontal impact: maps of the final distribution of the (equivalent) plastic strain (a) in the PC and (b) in the EPS.

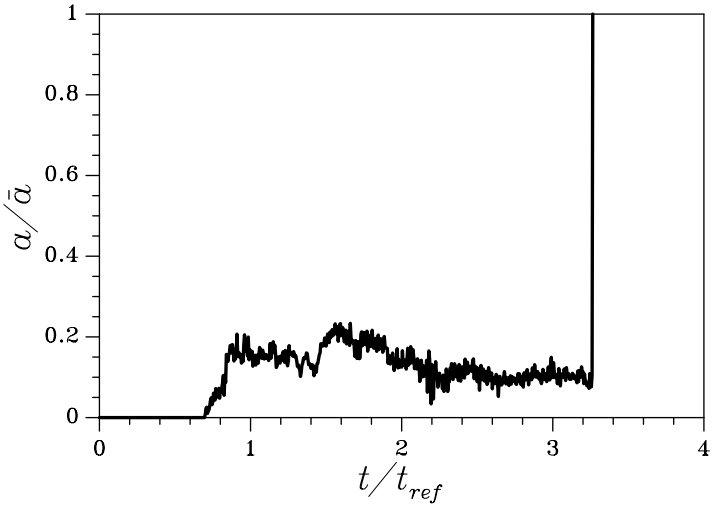

Figure 13. Back impact: numerical acceleration history of the headform.

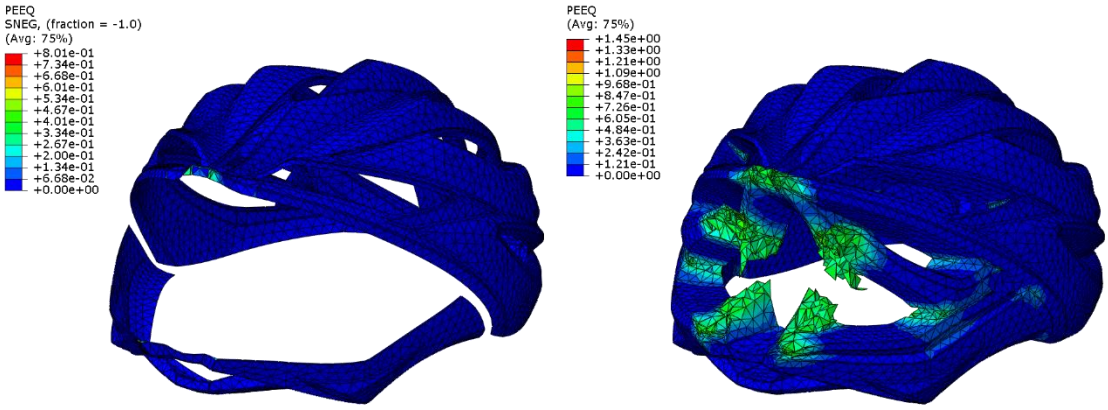

(a) (b)

Figure 14. Back impact: maps of the final distribution of the (equivalent) plastic strain (a) in the PC and (b) in the EPS.

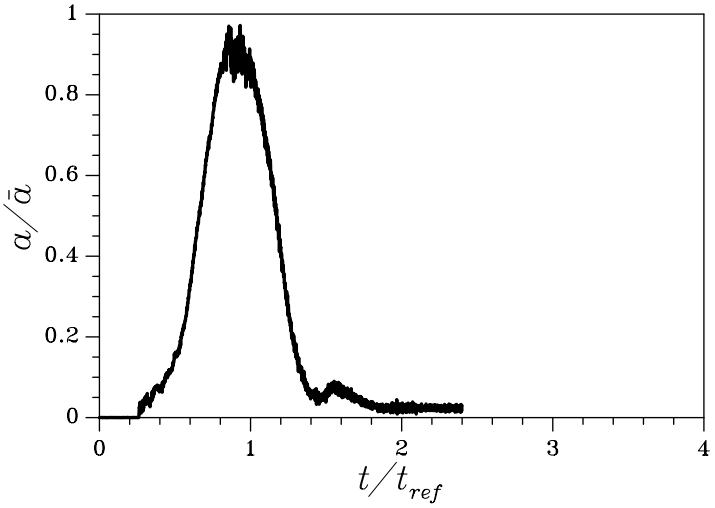

Figure 15. Lateral impact: numerical acceleration history of the headform.

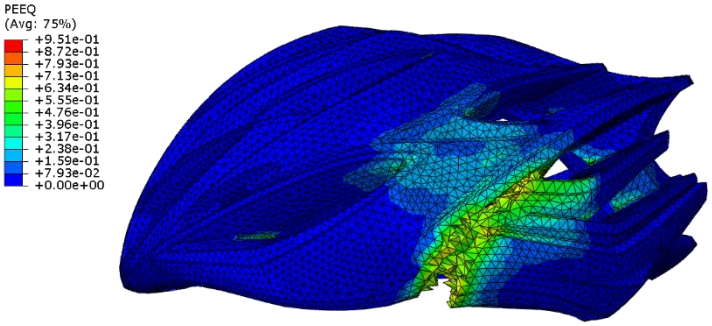

Figure 16. Lateral impact: map of the final distribution of the (equivalent) plastic strain in the EPS.